High rates of rock organic carbon oxidation sustained as Andean sediment transits the Amazon foreland-floodplain

Mathieu Dellinger[1,2] *, Robert G. Hilton[1,3], J. Jotautas Baronas[4], Mark A. Torres[5], Emily I. Burt[6], Kasey E. Clark[7], Valier Galy[8], Adan Julian Ccahuana Quispe[9], A. Joshua West[6]

[1] Department of Geography, Durham University, Durham, DH1 3LE, UK
[2] EDYTEM-CNRS-University Savoie Mont Blanc (USMB), Chambéry, 73000, France
[3] Department of Earth Sciences, University of Oxford, Oxford, OX1 3AN, UK
[4] Department of Earth Sciences, Durham University, Durham, DH1 3LE, UK
[5] Department of Earth, Environmental, and Planetary Sciences, Rice University, Houston, TX, USA
[6] Department of Earth Sciences, University of Southern California (USC), Los Angeles, CA, 90089, USA
[7] Department of Geography & Planning, University of Liverpool, Roxby Building, Liverpool, L69 7ZT, UK
[8] Department of Marine Chemistry and Geochemistry, Woods Hole Oceanographic Institution, Woods Hole, MA, 02543, USA
[9] Escuela Profesional de Biologia, Facultad de Ciencas, Universidad Nacional de San Antonio Abad del Cusco, Cusco 08000, Peru

***Email:** mathieu.dellinger@univ-smb.fr

Author Contributions:

MD, RGH and AJW designed the research and obtained funding. All authors contributed to fieldwork and sample collection. MD undertook the geochemical analysis of materials for this work. MD analyzed and interpreted the data with RGH. MD and RGH wrote the manuscript with input from all authors.

Competing Interest Statement:

The authors declare no competing interests.

Classification:

Earth, Atmospheric, and Planetary Sciences

Keywords:

Carbon cycle; weathering; rivers; Amazon; Andes; Organic carbon

Abstract

The oxidation of organic carbon contained within sedimentary rocks ("petrogenic" carbon, or hereafter OC_{petro}) emits nearly as much CO_2 as is released by volcanism, thereby playing a key role in the long-term global C budget. High erosion rates in mountains have been shown to increase OC_{petro} oxidation. However, these settings also export un-weathered material that may continue to react in downstream floodplains. The relative importance of OC_{petro} oxidation in mountains versus floodplains remains difficult to assess as disparate methods have been used in the different environments. Here, we investigate the sources and fluxes of rhenium (Re) in the Rio Madre de Dios to quantify OC_{petro} oxidation from the Andes to the Amazon floodplains using a common approach. Dissolved rhenium concentrations (n=131) range from 0.01 to 63 pmol.L^{-1} and vary depending on lithology and geomorphic setting. We find that >75% of the dissolved Re derives from OC_{petro} oxidation and that this proportion increases downstream. We estimate that in the Andes, OC_{petro} oxidation releases $11.2^{+4.5}/_{-2.8}$ tC km^{-2} yr^{-1} of CO_2, which corresponds to ~41% of the total OC_{petro} denudation (sum of oxidized and solid OC_{petro}). A Re mass balance across the Rio Madre de Dios shows that 46% of OC_{petro} oxidation takes place in the Andes, 14% in the foreland-lowlands, and 40% in the Andean-fed floodplains. This doubling of OC_{petro} oxidation flux downstream of the Andes demonstrates that, when present, floodplains can greatly increase OC_{petro} oxidation and CO_2 release.

Significance Statement:

Erosion and weathering play key roles in Earth's carbon cycle, controlling climate over millions of years by transferring CO_2 to and from the atmosphere. Weathering of sedimentary rocks in mountains can release CO_2 when ancient organic carbon in rocks is chemically broken down. However, mountain erosion also moves rock organic carbon that has not been broken down and is transported by rivers to lowland floodplains to an unknown fate. Here we use rhenium in rivers to quantify rock organic carbon weathering in the Andes and adjacent floodplain. Erosion in the Andes leads to high rates of CO_2 release. However, CO_2 release doubles when including the floodplains. The presence or absence of floodplains next to mountains governs CO_2 release by weathering.

Main text:

Introduction

Substantial climatic changes have occurred throughout geologic time, with the evolution of the carbon cycle and the planet's habitability modulated by the interplay between tectonic, climatic, erosional and biological processes. Over long timescales (>10^5 years), the abundance of CO_2 in the atmosphere is determined by the balance of the major carbon sources and sinks (1). It has been widely debated how the Earth system responds to transient imbalances in the long-term carbon (C) cycle, with much focus of prior research on the CO_2 sink associated with the chemical weathering of silicate minerals (1, 2). However, recent studies have highlighted the potential importance of changes in CO_2 fluxes linked to oxidative weathering (OW) reactions of sedimentary rocks on the continents (3–5). Although receiving less attention to date, OW of reduced phases in sedimentary rocks is central to both the C and O cycles (6, 7). Carbon dioxide release and O_2 consumption can result from both (i) oxidation of fossil (i.e. "rock-derived" or "petrogenic") organic matter (OC_{petro}) and (ii) the OW of sulfides that produces sulfuric acid, which can be neutralized by carbonate minerals, or by the carbonate buffer of continental waters leading to net CO_2 release to the atmosphere (8, 9).

The export of particulate OC_{petro} by rivers in their sediment load has been documented in many places (10–16), but only a few field-based studies have estimated the rate of OW of

OC_{petro} (3). The highest fluxes of OW of OC_{petro} (reported as a yield per catchment area, of 5 to 30 $tC.km^{-2}.yr^{-1}$) have been measured in small high standing islands composed of sedimentary rocks such as in Taiwan (17) and New Zealand (4), as well as in catchments from major mountain ranges (0.5 to 5 $tC.km^{-2}.yr^{-1}$) like the Yamuna (18), Swiss Alps (19) and in the Mackenzie River basin (20). This reflects the role of physical erosion rate in mountains that can continuously supply OC_{petro} to oxygenated surface waters and the atmosphere (17, 21). A consequence is that, in combination with carbonate weathering by sulfuric acid, CO_2 release by OC_{petro} oxidation can be larger than CO_2 consumption by silicate weathering in many erosive settings (3), challenging the idea that chemical weathering in mountain belts is a long-term carbon sink (22–24).

While physical erosion can enhance the supply of reduced phases to OW reactions and increase the weathering flux (8, 17, 25), the overall intensity of weathering can also decline (26), meaning that erosive catchments can also export very large amounts of 'unweathered' particulate OC_{petro} (7). These particulate fluxes can be very high, for instance reaching 250 $tC.km^{-2}.yr^{-1}$ (13, 26). The subsequent fate of this material is critical to governing how physical erosion and weathering impact the carbon cycle. It has been proposed (10, 14) that this OC_{petro} can be largely oxidized in floodplains when present (e.g. in the Amazon and Ganges floodplain), because of the long residence time of sediments and the warm and oxidative conditions that prevail in the floodplains relative to upstream mountainous area. Hence, the mountain catchments underlain by sedimentary rocks with river floodplains could have greater net CO_2 release from OW than mountain catchments without floodplains. Over 10^5-10^6 year timescales, the configuration of continental drainages can shift dramatically (27) and young, high standing mountain ranges potentially operate differently in terms of OW and CO_2 release relative to mountain ranges with floodplain drapes.

Despite the recognition of these geomorphological controls on OW (3), the relative contributions of mountain versus floodplain weathering to OC_{petro} oxidation and CO_2 release remains unknown. This knowledge gap arises in part because different methods have been used to assess OW of OC_{petro} in mountain catchments (4, 17) versus floodplains (10, 14). In mountain catchments, dissolved rhenium (Re) fluxes have been used for quantifying OC_{petro} oxidation fluxes (17), whereas studies on floodplains have used sediment fluxes and radiocarbon content of river sediments (Bouchez et al., 2010). Both methods have benefits and drawbacks. Dissolved Re fluxes are easier to measure because water discharge is usually known with more precision than sediment flux. On the other hand, there are large uncertainties on the source of dissolved Re and on the estimation of the Re/OC_{petro} ratio of the bedrock (20). Because water and sediments integrate over different spatial and temporal scales, their direct comparison can also be problematic. Overall, the influence of floodplains on the global OC_{petro} budget remains an open question (3, 28).

To resolve these issues, here we investigate the source and fluxes of dissolved and particulate rhenium (Re) in the Madre de Dios watershed, part of the larger Amazon Basin. We focus on an elevation transect ranging from the high Andes to the low-elevation floodplains and use Re to quantify the flux of CO_2 released by OC_{petro} oxidation. These catchments have been well-characterized by previous studies in terms of erosion rates and their major dissolved load (11, 23, 29), and benefit from time-series samples over a range of river discharges. Most importantly, this setting provides an opportunity to determine the rate of OC_{petro} oxidation in each of the different geomorphological settings (mountain, foreland, floodplain) within a single river basin.

Study site

The Madre de Dios watershed (124,231 km^2 at the confluence with the Rio Beni in Bolivia) is one of the main headwaters of the Amazon basin (30), the largest river basin in the world. The precipitation in the Madre de Dios region is between <1000 and >6000 mm.yr^{-1} and the mean annual temperature varies with elevation from 4 to 25°C (30–32). The Rio Madre de Dios drains: i) the eastern flank of the Andes in Peru with elevations from 1300 m to 6300 m, ii) the mountain front with elevations from 500 m to 1300 m, iii) the foreland corresponding to elevations of less than 500 m, in which river basins are not Andean-fed but had undergone some recent uplift associated with the Fitzcarrald Arch, and iv) the Andean-fed floodplains, which are the low-relief environments adjacent to active river channels from rivers originating from the Andes and where sediments are deposited and exchanged with the main channel. The bedrock in the headwaters is primarily composed of Paleozoic and Mesozoic sedimentary and metasedimentary rocks (with $[OC_{petro}] \sim 0.4$ to 0.6%) and some minor granitic intrusions in the Andes (23). Observations from the neighboring Beni catchment with similar lithologies to the Madre de Dios show that this OC_{petro} is a mixture of disordered and graphitic carbon (10).

To characterize the spatial variability of dissolved Re concentrations ($[Re]_{diss}$) across the Madre de Dios River basin (Fig. 1A), we studied a large number of small tributaries draining each geomorphological setting that have been subject to prior work on water, sediment and carbonate and silicate weathering fluxes (11, 23, 29, 33–35). To characterize the dissolved Re sources, we sampled stream, spring and lysimeter waters from small first-order catchments in each geomorphological setting (referred as Wayqecha Small Catchment "WAY-SC", Villa Carmen Small Catchment "VC-SC" and CICRA Small Catchment "CICRA-SC"; Burt et al., 2022). To examine the downstream evolution of OC_{petro} weathering processes across these geomorphic settings, we studied in detail four main nested sub-catchments that define a geomorphic gradient from the Andes to the Foreland-floodplain: the Rio Kosñipata at Wayqecha in the Andes (referred as "WAY", altitude 2250 m); the Rio Kosñipata at San Pedro in the Andes ("SP", altitude 1360 m); the Alto Madre de Dios at Manu Learning Center ("MLC", altitude 479 m) at the transition between the Andes and the Foreland; and the Madre de Dios at CICRA-Los Amigos research station ("CICRA", altitude 217 m). Time series $[Re]_{diss}$ and discharge data from the years 2010-2011 are used to characterize changes in Re concentration during the hydrological cycle. The measured annual runoff for the year 2010-2011 was 3065 mm.yr^{-1} at the "WAY" site (Upper Andes) to 2796 mm.yr^{-1} at SP. The suspended sediment flux (a proxy for erosion rate) at San Pedro (SP) measured during the same period is 3500 t.km^{-2}.yr^{-1} (11), similar to the estimated suspended sediment load from the Andean area of the entire Madre de Dios watershed (3208 t.km^{-2}.yr^{-1}; 35). Finally, to integrate weathering processes over large areas and establish a Re mass-budget, we studied several large tributaries with Andean-fed floodplains that drain all geomorphic settings (Rios Manù, Colorado, Chiribi, Inambari and Tambopata).

Results

Rhenium concentrations were measured on water samples collected from several field campaigns, including (i) from the Madre de Dios mainstem and major tributaries sampled unders different flow conditions in 2012 and 2013 (23, 34, 38), and again at high and low flow in March and May 2019 (35), (ii) from time-series samples collected at four nested catchment sites (areas 50 to 27 830 km^2) in 2010 and 2011 at various hydrological conditions (29, 33), and (iii) from another time series of samples collected from smaller first-order catchments (<1 km^2 area) across the elevation gradient (36). The time-series dataset is used to characterize the relationship between Re concentration and instantaneous runoff.

Spatial variability of dissolved Re concentrations

Rhenium concentrations in dissolved samples (n=133) range from 0.01 to 63 pmol.L^{-1}, with spatial variability depending on the sample type, bedrock lithology and geomorphic setting (Fig. 1B; Dataset S1). Rivers have $[Re]_{diss}$ ranging from 0.1 to 9.5 pmol.L^{-1}. The rainwater sample collected in the Andes has $[Re]_{diss}$ below detection limit ($[Re]_{diss} < 0.05$ pmol.L^{-1}) while

$[\text{Re}]_{\text{diss}}$ in the throughfall sample from the same location is 0.36 pmol.L^{-1}. Lysimeter samples from first-order small catchments in the Andes and in the Foreland have also very low $[\text{Re}]_{\text{diss}}$, ranging from 0.09 to 0.12 pmol.L^{-1} (n=4). In contrast, the two hot springs samples from Aguas Caliente have very high $[\text{Re}]_{\text{diss}}$ (39 pmol.L^{-1} and 63 pmol.L^{-1}). However, the $[\text{Re}]_{\text{diss}}$ of the Alto Madre de Dios downstream of the hot springs is unchanged compared to $[\text{Re}]_{\text{diss}}$ upstream of the hot springs, suggesting that their contribution to the Re budget is negligible.

In terms of lithology, small rivers draining mostly granitic rocks in the High Andes have lower Re concentrations (0.56±0.44 pmol.L^{-1}, 1σ, n=6) than rivers draining sedimentary rocks (2.90±2.06 pmol.L^{-1}, 1σ, n=25). Rivers draining the mountain front composed of mostly granites also have lower $[\text{Re}]_{\text{diss}}$ (1.32 pmol.L^{-1}, n=2) than those draining sedimentary rocks (3.88±1.12 pmol.L^{-1}, 1σ, n=10).

We observe a notable geomorphic control on $[\text{Re}]_{\text{diss}}$ for the tributaries and first-order catchments draining specific settings, but not for the nested catchments (Fig. 1B). Tributaries draining sedimentary rocks in the High Andes and Mountain front have significantly higher $[\text{Re}]_{\text{diss}}$ (3.22±1.82 pmol.L^{-1}, 1σ, n=38) than those draining the foreland (0.70±0.53 pmol.L^{-1}, 1σ, n=9). For first-order catchments, $[\text{Re}]_{\text{diss}}$ is the highest in the High Andes (0.12 to 0.48 pmol.L^{-1}), as compared to <0.15 pmol.L^{-1} in the Mountain front and Foreland. In contrast, no significant change in $[\text{Re}]_{\text{diss}}$ downstream is observed for nested catchments, although the average concentration at WAY (3.76±0.76 pmol.L^{-1}, 1σ, n=6) is slightly higher than at the SP site (2.59±0.44 pmol.L^{-1}, 1σ, n=7). We note that in March 2019, $[\text{Re}]_{\text{diss}}$ was higher (4.22 pmol.L^{-1}) at SP than the average $[\text{Re}]_{\text{diss}}$ of time-series measurements from the 2010-2011 period, perhaps related to a large landslide in this catchment in the intervening period. At the foreland-floodplain site (CICRA), $[\text{Re}]_{\text{diss}}$ = 3.69±0.98 pmol.L^{-1} (1σ, n=9). For the main tributaries of the Madre de Dios, we observe the highest $[\text{Re}]_{\text{diss}}$ in the Manù (1.5 to 9.5 pmol.L^{-1}), lowest $[\text{Re}]_{\text{diss}}$ in the Chiribi and Colorado rivers (0.5 to 2.2 pmol.L^{-1}), and intermediate $[\text{Re}]_{\text{diss}}$ in the Alto Madre de Dios (3.4 to 4.7 pmol.L^{-1}), Inambari (3.3 pmol.L^{-1}) and the Tambopata (2.3 pmol.L^{-1}).

Temporal variability of dissolved Re concentrations

In the four nested-catchments, $[\text{Re}]_{\text{diss}}$ generally decreases with increasing instantaneous runoff, Q, except for the high-altitude Andean site (WAY) where $[\text{Re}]_{\text{diss}}$ shows no clear relationship with runoff (Fig. 1C). The relationship can be modeled using a power law $[\text{Re}]_{\text{diss}} = a \times Q^{b}$, with a and b as the two fitted constants. For our samples, we observe a decrease of the b value from the Andes (–0.09±0.12 in WAY, –0.15±0.08 in SP; 1σ) to the mountain front (–0.40±0.06 in MLC) and the foreland-floodplain (–0.46±0.08 in CICRA), indicating a more chemostatic behavior of Re in the Andes, and more dilutional behavior in the Foreland-floodplain. This decrease of the b value with elevation is similar to that observed for most major elements (29).

Re concentrations in solids

The Re concentration in bedloads ($[\text{Re}]_{\text{BM}}$) from Andean rivers draining shales ranges from 0.12 to 0.50 ppb with an average of 0.28±0.06 ppb (±2SE, n=14; Fig. 2). These are higher than the Re concentration in Andean soil samples (39) collected close the SP site 0.07±0.07 ppb (±2SE, n=3) and in the Foreland-floodplain 0.04±0.01 ppb (±2SE, n=4). The $[\text{Re}]_{\text{BM}}$ is slightly higher in WAY (0.31 to 0.36 ppb) compared to SP (0.23 to 0.26 ppb). Two rock samples were analyzed: [Re] of the OC_{petro} and sulfur-rich sedimentary rock sample is almost 100 times higher (4.61 ppb) than the igneous rock (0.06 ppb). The [Re]/[OC] ratio in bedloads and rocks vary from 0.27×10^{-7} to 2.65×10^{-7} g.g^{-1} with an average of $0.93\pm0.38\times10^{-7}$ g.g^{-1} (±2SE, n=16; Fig. 2). The average [Re]/[OC] for the Kosñipata stream (WAY and SP sites) is $0.80\pm0.12\times10^{-7}$ g.g^{-1} (±2SE, n=5). This [Re]/[OC] ratio value is similar to bedload from New Zealand Southern Alps

(4) but lower than bedloads from Taiwan (17), the Yamuna River (18) and the Mackenzie River (20).

Discussion

Our aim is to determine the rates and controls of OW of OC_{petro} across the transition from the Andes Mountains to Amazon floodplain in the Madre de Dios basin. To do so, we need to characterize the source, behavior, and fluxes of dissolved Re. Following previous studies (4, 17, 19, 20, 40), the OC_{petro} oxidation yield ($J_{OCpetro\text{-}ox}$, tC km^{-2} yr^{-1}) can be estimated from:

$$J_{OCpetro\text{-}ox} = J_{Re} \times f_C \times ([OC]/[Re])_{solids} \times (1 - f_{graphite}) \quad \textbf{[1]}$$

Where "J_{Re}" is the dissolved Re yield (in g km^{-2} yr^{-1}), the product of the Re concentration and runoff ($J_{Re} = [Re]_{diss} \times Q$), while "$([OC]/[Re])_{solids}$" is the OC/Re ratio in sedimentary rocks being weathered (in g.g^{-1}), "f_C" is the fraction of dissolved Re deriving from the oxidation of OC_{petro} and "$f_{graphite}$" is the proportion of graphite in the rocks that may be resilient to OW (14).

Dissolved Re source and yield

To determine the OC_{petro} oxidation flux using the Re proxy, we must first quantify the proportion of dissolved rhenium derived from OC_{petro} oxidation relative to other potential Re sources (rainwater, carbonates, sulfides, silicates, carbonates; ref.18). Following the approach developed in ref. (20), we use the $[Re]/[SO_4^*]$ and $[Re]/[Na^*]$ ratios to do so ($[Na^*]$ and $[SO_4^*]$ are concentrations corrected for atmospheric-derived contributions). In general sulfides have low Re/SO_4 (41) and silicates low Re/Na relative to OC_{petro} (20), and both Na and SO_4 are conservative soluble species in the Madre de Dios catchment (34, 35, 38). In analogy with studies on silicate and carbonate weathering, here we use local constraints on the end member compositions, using the combination of water samples from first-order catchments and tributaries (e.g. refs. 39, 40), combined with river sediments and rocks (23, 44) (Materials and Methods).

We find that small Upper Andes tributaries draining shales have a large range of $[Re]/[SO_4^*]$ and $[Re]/[Na^*]$ ratios that can be interpreted as a mixing trend between sulfides and OC_{petro} weathering, with limited Re contribution from silicate weathering (Fig. 3). In contrast, Andean tributaries draining granites, and rivers draining the foreland, have ratios that can be mostly explained by a mixture between silicates and OC_{petro} (Fig. 3). A mixing analysis (Materials and Methods) shows that the fraction of dissolved Re derived from OC_{petro} oxidation, f_c (Equation 1), is >0.75 in the Andes (sites WAY and SP) and increases downstream to >0.90. Seasonal variability of the Re source is small but significant (less than 20% variability), with higher proportion of Re derived from OC_{petro} oxidation in the Andes at higher runoff. This could reflect the larger contribution of shallow groundwaters from the unsaturated zone above the sulfide OW front (19). The fraction of Re derived from sulfide OW decreases from ~0.15-0.25 in the Andes (WAY and SP) to <0.05 in the Foreland-floodplain (CICRA). The fraction of Re derived from silicate weathering is generally <0.05 but reaches ~0.2 for rivers draining only the foreland (e.g. Los Amigos River). Altogether, this shows that in the Madre de Dios basin, the majority of dissolved Re is derived from OC_{petro} oxidation, confirming observations in other catchments where sedimentary rocks dominate the geology (19, 20, 45).

Calculation of dissolved Re yield (J_{Re}) can be done in several ways, i.e. using average $[Re]_{diss}$ (4, 17, 18, 46), discharge-weighted average $[Re]_{diss}$ (41) or rating curve-derived $[Re]_{diss}$ (19) and annual or instantaneous water discharge estimates. Here, these methods return similar results (Materials and Methods; Dataset S3). Therefore, we take advantage of paired $[Re]_{diss}$ and discharge measurements (at the four nested catchment sites and at the main tributaries) and use discharge-weighted average $[Re]_{diss}$ and annual water discharge to derive dissolved Re yield. For the main tributaries, the highest J_{Re} is in the Manu River catchment ($2.0^{+0.9}/_{-0.7}$ g km^{-2} yr^{-1}) and the lowest for the Las Piedras river (0.3±0.1 g km^{-2} yr^{-1}). For the nested catchments, the Re yield is 2.1±1.0 g km^{-2} yr^{-1} and 1.3±0.2 g km^{-2} yr^{-1} for WAY and SP sites respectively, and 1.6±0.4 g km^{-2} yr^{-1} for the Foreland-floodplain (CICRA) site. Although there is slight decrease with elevation, the main result is that the specific Re yield of the Rio Alto Madre de Dios does not change, within uncertainty, when the Rio Alto Madre de Dios (Andes) reaches the Foreland-Floodplains.

Rates and control of OC_{petro} oxidative weathering in the Andes

We compute the OC_{petro} oxidative weathering rate (Equation 1) using the parameter values defined above (Dataset S3). As we have no constraint on $f_{graphite}$ in this setting, we do not account for this term here. To estimate the uncertainties, we use Monte Carlo simulations with 10 000 resolutions of the equation with distribution sampling of values within the errors of each parameter (4). The estimated OC_{petro} oxidative weathering fluxes based on dissolved Re yield are $16.7^{+11.9}/_{-8.8}$ tC km^{-2} yr^{-1} for the WAY site and $11.2^{+4.5}/_{-2.8}$ tC km^{-2} yr^{-1} for the SP site. The lower uncertainty on the $J_{OCpetro\text{-}ox}$ for SP is due to a higher precision on the water flux at this site (33).

It has been proposed that physical erosion rate is a major control on the rate of OW (3, 8), with a potential role for landslide erosion supplying fresh mineral surfaces (24). The present-day erosion rate of the Rio Kosñipata is high, with values between 1200 and 3500 t.km^{-2}.yr^{-1} (11) and frequent landslides (47). The $J_{OCpetro\text{-}ox}$ for the Kosñipata are much higher than in the Mackenzie (0.45 to 1.01 tC km^{-2} yr^{-1}) and the Swiss Alps (3.6 to 5.7 tC km^{-2} yr^{-1}) characterized by lower erosion rates, and more similar to rivers in New Zealand and Taiwan (4 to 30 tC km^{-2} yr^{-1}) which have higher erosion rates (3). Results from this study thus confirm the general control of erosion rate on the rate of OC_{petro} oxidation (3), though other factors can also play an important role (3, 48). The un-weathered solid OC_{petro} export at the SP site has been determined previously to be 16.1±1.4 tC.km^{-2}.yr^{-1} using sediment samples collected across the same time period (11). These fluxes imply that 41±10% of the total bedrock OC_{petro} is oxidized in the Andes, and the remainder is exported downstream. This OC_{petro} weathering intensity value is slightly lower than in the Mackenzie River basin (50%), similar to the Swiss Alps (19) and higher than in Taiwanese rivers (<20%) (17).

Our estimate of the flux of OC_{petro} oxidation in the Rio Kosñipata is the first attempt to quantify the CO_2 emission from weathering of OC_{petro} in the Andes. This estimate can also be compared with other carbon fluxes relevant to the long-term carbon cycle in the Andes in the Kosñipata catchment. In the SP catchment, the rate of biospheric organic carbon (OC_{bio}) export in river suspended sediments is 12.6±0.4 tC km^{-2} yr^{-1} (11), which is slightly higher than the OC_{petro} oxidative weathering yield. At the same site, the yield of carbon release associated with carbonate weathering by sulfuric acid is ~ 6 tC km^{-2} yr^{-1} (23), 45% lower than the rate of CO_2 release by OC_{petro} oxidation. Together, the OW of reduced phases (OC_{petro} and sulfides) in Andean sedimentary rocks release about 17 tC km^{-2} yr^{-1} to the atmosphere, confirming that OW of sedimentary rocks in mountain belts is a large source of CO_2 to the atmosphere.

Oxidative weathering in the foreland and in the Andean-fed floodplains

Once the OC_{petro} that survived OW in the Andes has reached the foreland and the floodplains, it can undergo further OW during transport and deposition in the floodplains (10). It has been suggested that this process can be a large source of CO_2 to the atmosphere in the neighbouring Beni catchment (10) and in the Ganges floodplain (14). Here we take several approaches to isolate the weathering signal from the foreland (here defined as <500 m) versus the Andean-fed floodplain (<500 m and low relief adjacent to active river channels where Andean-derived sediments are exchanged). First, we assess the OC_{petro} weathering flux in the foreland by using data from the Las Piedras river catchment, since it drains the foreland exclusively with no Andean contribution. The $[\mathrm{Re}]_{\mathrm{diss}}$ concentration at Las Piedras (1.24 ± 0.35 pmol.L^{-1}, 2SE) is low like the two other medium-size foreland rivers, the Blanco (0.36 ± 0.06 pmol.L^{-1}) and the Los Amigos (0.50 ± 0.16 pmol.L^{-1}). The [Re]/[OC] ratio of bedrock in Las Piedras can be reasonably assumed to be equivalent to the Andean-derived bedload from the Rio Kosñipata, given that the foreland-floodplain region is predominantly underlain by Andean-derived sediments (23). Using this, we calculate a $\mathrm{J}_{\mathrm{OCpetro\text{-}ox}}$ of $1.9^{+1.2}/_{-0.8}$ tC.km^{-2}.yr^{-1} which is about 6 times lower than in the Andes and similar to the rate measured in the Mackenzie River basin (20).

To estimate the $\mathrm{OC}_{\mathrm{petro}}$ weathering flux in the floodplains, we attempt a mass-balance at the scale of the whole Madre de Dios catchment (118 459 km^2 at El Sena station near Riberalta, Ref. 36). Assuming the $J_{\mathrm{OCpetro\text{-}ox}}$ from SP (Upper Andes) is representative of the Andean area (40 868 km^2; defined as <500 m) of the Madre de Dios, we calculate a total Andean $J_{\mathrm{OCpetro\text{-}ox}}$ of $0.46^{+0.18}/_{-0.11}$ MtC.yr^{-1}. This assumption is justified as the SP catchment has similar erosion rates as the inferred Andean erosion rate for the whole Madre de Dios River (37). The contribution from foreland weathering (< 500m; 77 591 km^2) can be estimated using the $J_{\mathrm{OCpetro\text{-}ox}}$ from the Las Piedras River (19 630 km^2) as $0.15^{+0.09}/_{-0.06}$ MtC.yr^{-1}. The total $J_{\mathrm{OCpetro\text{-}ox}}$ at the mouth of the Madre de Dios is $1.00^{+0.43}/_{-0.28}$ MtC.yr^{-1}. Hence, the contribution of Andes + Foreland is lower than the total $J_{\mathrm{OCpetro\text{-}ox}}$ of the Madre de Dios at its mouth by $0.39^{+0.16}/_{-0.11}$ MtC.yr^{-1}, which we attribute to weathering in the floodplain. This mass-balance indicates that ~46% of the total $\mathrm{OC}_{\mathrm{petro}}$ oxidation takes place in the Andes, ~40% in the floodplains, and ~14% in the foreland-lowlands (Fig. 4A).

The deposition and weathering of sediments in the floodplain constitutes a different mechanism compared to upland weathering (29, 49). Sediment and water exchange and storage during floodplain transit by rivers can result in long sediment residence times (50), and influence water flux, and redox state, which could all facilitate OW (7). In addition, the warmer climatic conditions in the floodplain relative to the Andes could be important in setting reaction rates (21), while the length of floodplains and their channel migration rates (51) could also be important controlling variables. Scaled laboratory experiments have been used to suggest that in-situ oxidation during within river transport is small (52) meaning reactions in sediment stores of floodplains are likely to be of most importance (53).

Our paired instantaneous $[\mathrm{Re}]_{\mathrm{diss}}$ and discharge measurements from the same sampling trips (in 2013 and 2019, both wet and dry seasons) covering both upstream and downstream floodplain sections constrain the location of $\mathrm{OC}_{\mathrm{petro}}$ oxidation reactions in the floodplains between MLC and CICRA (Fig. 4B). The ~85 km long section of the river along the course of the Alto Madre de Dios floodplain, between the Mountain Front (MLC) and the confluence with the Rio Manu, is mostly braided and multi-channel, with mobile channel bars comprised of sand and fine gravel. Measurements show a significant increase of J_{Re} (Re flux). Water isotopes indicate lack of significant water, and therefore likely Re, contribution from tributaries in this river reach (see Materials and Methods). Hence, we attribute this J_{Re} increase (from 4 to 30%, Fig. 4B) to weathering of $\mathrm{OC}_{\mathrm{petro}}$ from Andean sediments transiting in the floodplains (SI Appendix). The same calculation can be done using mean annual Re flux, but with a larger uncertainty. We calculate that the mean annual J_{Re} increases by $31\pm20\%$ which corresponds to a flux of CO_2 release through $\mathrm{OC}_{\mathrm{petro}}$ oxidation in the floodplain reach between MLC (Mountain front) and AMdD of 0.03 ± 0.01 MtC.yr^{-1}. In comparison, the CO_2 release through $\mathrm{OC}_{\mathrm{petro}}$ oxidation in the Andean part of the Alto Madre De Dios catchment is 0.08 ± 0.02 MtC.yr^{-1}. As the solid $\mathrm{OC}_{\mathrm{petro}}$ load at MLC is 0.12 ± 0.01 MtC.yr^{-1} (Ref. 32, assuming similar solid $\mathrm{OC}_{\mathrm{petro}}$ yield as at SP), this would suggest that ~25% of Andean-derived solid $\mathrm{OC}_{\mathrm{petro}}$ is oxidized before reaching the confluence with the Rio Manu over a floodplain length of 85 km.

In contrast, in the section between AMdD and CICRA (~180 km long), where a larger, single channel meanders through the floodplain, we observe no significant Re flux increase in wet seasons (2013 and 2019) and dry season 2019. For the dry season in 2013, we even observe a small decrease of Re yield along the section (Fig. 4B). Similarly, using mean annual J_{Re}, we calculate no significant increase in OC_{petro} oxidation, within uncertainties (Fig. 4B, SI Appendix), in this section nor in the CICRA-PM section (~170 km long). Over the transit from MLC to CICRA, the isotopic composition of sulfate suggests minimal sulfate reduction (36), suggesting that oxygen is available for OW weathering along this river reach. In addition, the warm tropical climate could drive higher reaction rates and OC_{petro} oxidation (21). Therefore, the apparent limited floodplain weathering could reflect an exhaustion of reactive OC_{petro} supplied from Andean erosion upstream. Regardless of the mechanisms at play, the Rio Madre de Dios example shows that high rates of OC_{petro} oxidation in the mountain headwaters can be matched by OW in the foreland (Fig. 4). A large proportion of floodplain weathering appears to happen over a relatively short-length scale (~<85 km) after exiting the Andes.

Finally, for the section furthest downstream, PM-Ribe (~560 km long), calculation using mean annual J_{Re} show a 10% increase in Re flux. This may reflect OW of reactive OC_{petro} supplied by the Inambari and/or the Tambopata, in combination with a longer time sediments spend in this long floodplain section (e.g. see ref. 50). Yet, this observation should be interpreted with caution due to the large uncertainty (±13%) associated with our calculation. Additional work on this part of the catchment is necessary to refine these calculations.

Implications for the long-term carbon cycle

Previous studies on the Amazon River found significant CO_2 release from OC_{petro} oxidation during the transit of fluvial sediments in the Madeira floodplain (10, 11). They found that the solid OC_{petro} flux from the Madeira at the confluence with the Amazon is much lower than the solid OC_{petro} supplied by the Beni at the mountain front and transported through the plain. They estimated a CO_2 emission of 0.50 $MtC.yr^{-1}$ across the Rio Beni floodplain. Our Re-based estimate of OC_{petro} oxidation during the transit of Madre de Dios sediments in the floodplain ($0.39^{+0.16}/_{-0.11}$ $MtC.yr^{-1}$) is of similar magnitude. The total CO_2 emission from OC_{petro} oxidation in the whole Madre de Dios catchment ($1.00^{+0.43}/_{-0.28}$ $MtC.yr^{-1}$) is more than twice the silicate weathering CO_2 drawdown ($0.43^{+0.22}/_{-0.09}$ $MtC.yr^{-1}$; ref. 53). Considering that sulfide oxidation also contributes to the carbonate weathering flux (23), the net CO_2 balance during weathering in the Madre de Dios catchment appears to be tipped firmly toward being a CO_2 source (3).

Our findings from the Rio Madre de Dios catchment allow us to postulate a broader role for floodplain weathering in enhancing the CO_2 release by OC_{petro} oxidation. Uplift and exhumation of sedimentary rocks in a mountain range can increase the supply of OC_{petro} to an oxygenated weathering zone (17, 21) and increase the rates of OC_{petro} oxidation and CO_2 release, as we observe in the Andes (Fig. 4). However, the overall weathering intensity can be low, with only ~20% to 50% of OC_{petro} oxidized, meaning there is further potential for CO_2 release. On high standing mountain islands, floodplains are short. For instance, in Taiwan rivers have floodplains <40 km long, and many are shorter than 5 km, and there un-weathered OC_{petro} is re-buried offshore (16). However, if the tectonic setting permits the growth of a larger continental floodplain, additional OC_{petro} oxidation is very likely to occur even if just ~100 km in length based on our findings (Fig. 4). In this case, only extremely refractory OC_{petro} escapes oxidation (10). While future work will need to establish how temperature and O_2-supply impact OC_{petro} oxidation rates in floodplains (7, 21), our results suggest that the formation of floodplain adjacent to a mountain range allows more complete OC_{petro} oxidation during sediment transit. Over multi-million year timescales, the growth and waning of riverine floodplains and continental sediment storage (27) could thus act as a powerful carbon cycle modifier throughout Earth's history.

Materials and methods

The materials and methods are summarized here; further details are provided in SI Appendix. All data used in this study are reported in Datasets S1–S5.

Sample collection and discharge measurements. Major cation and anion concentration data of samples from 2010 to 2013 are from Torres et al., (2015, 2016). Detailed information on the sampling protocol can be found in those studies. In summary here, for the four main nested catchment sites (WAY, SP, MLC and CICRA, Fig. 1), time-series samples were collected between 2010 and 2011 using a clean PP bottle and filtered on site with 0.2 µm porosity nylon filter (29). At these sites, water discharge was measured at the same time as sampling by monitoring water levels manually and converting to discharge using a rating curve. At the SP site, river level was monitored with a water level logger that recorded river level measurements every 15 min (33). At other localities, samples were collected on fieldtrips in 2012, 2013, 2016 and 2019 (Dataset S1). Water samples were collected from the river surface using clean bucket and transferred to 10 or 20 L plastic bags before filtration. Samples were filtered within 24 to 48h of collection with 0.2µm porosity polyethersulfone (PES) filters. The discharge ("Q") at CICRA was measured during each sampling trip using an Acoustic Doppler Current Profiler (ADCP, RD1 Sentinel GED154 in March 2013 and SonTek M9 in August 2013 and in March and May 2019). In 2019, the discharge of the Alto Madre de Dios, Rio Manù, Chiribi and Colorado were also measured by ADCP. All discharge measurements are from Torres et al., (2017) and Burt et al., (2021)

Re concentration measurements in water and sediments. The dissolved Re concentrations were measured following the same protocol as described in ref. (19). Briefly, dissolved Re concentrations ($[Re]_{diss}$) were measured by direct calibration against a set of seven standards with varying Re abundances and similar matrixes to river water, by quadrupole inductively coupled plasma mass spectrometry (Q-ICP-MS, Agilent Technologies 7900). Calibration standards and samples were doped with 0.025 mg/L concentration of internal standard Tb and Bi to correct for instrumental drift and matrix drift. Accuracy and precision of the measurements was assessed by repeated measurements of various riverine standard reference materials, in particular reference materials SLRS-5 and SLRS-6 at various dilutions. The standards confirmed better than 10% accuracy and precision. For sediment samples, the rhenium concentrations were determined using the method in ref. (55). A mass of 0.2 to 0.5g was digested using a mixture of 3 mL 27M HF and 3 mL 16M HNO_3 for 24 to 48h at 120°C on a hot plate. Digested solutions were processed through AG1-X8 resin to separate Re from the rest of the matrix. Rhenium concentrations were then measured with a Neptune MC ICP-MS at Durham University.

Dissolved Re yield calculations. Several methods can be used to determine dissolved ion yields depending on the number of paired water discharge (Q) and concentration measurements, their frequency and the behavior of the element of interest in relation with discharge (56). Previous studies with large datasets of Re concentration and discharge (19, 20) have used a rating curve approach to quantify dissolved yields, by fitting power law functions to the trends in the data and using this relationship to predict predicted for each daily discharge value and annual fluxes. Other studies have used discharge-weighted average concentration (41) or average concentration of several measurements (4, 17, 18, 46) combined with annual water discharge estimates.

The four nested catchments in our dataset have between five and nine Q and $[Re]_{diss}$ data pairs for each catchment (Fig. 1C). For the large tributaries (Manu, Colorado, Chiribi, Alto Madre de Dios), our dataset includes 4 paired Q and $[Re]_{diss}$ measurements each. For all the sites, we use three different methods to calculate the Re yield and uncertainties: i) mean $[Re]_{diss}$ ±SE multiplied by annual discharge; ii) discharge-weighted mean $[Re]_{diss}$ ±SE multiplied by annual discharge; and iii) average of measured instantaneous Re fluxes, J_{Re} ±SE. The advantage of the first method is that it includes more $[Re]_{diss}$ measurements (since the instantaneous discharge was not measured for all samples). The disadvantage is that there is a potential bias toward high concentration by not weighting to discharge. The third method is useful if annual discharge is not known, however it has the disadvantage of being less accurate because instantaneous fluxes vary more than instantaneous concentrations (56). Discharge values and uncertainties are reported in Dataset (S3). For the WAY and SP catchments, we use annual discharge values from Clark et al., (2014), determined over the year 2010. In addition, we use average annual discharge values dataset for the main tributaries of the Madre de Dios that were determined by water balance over the period 1968-1982 (57). They calculate a total discharge at the mouth of the Madre de Dios (Riberalta) of 6369 $m^3.s^{-1}$ which are very close (only 12% higher) to the discharge measured during the 2002–2011 period (5661 $m^3.s^{-1}$; Vauchel et al., 2017). For CICRA, the discharge can be estimated by adding the annual discharge values of the Manu, Alto Madre de Dios, Colorado from Abastos Lara, (1987) and considering that the Rio Chiribi contributes 7.5% of the total discharge in CICRA (see Dataset S5). This gives a value of 2165 $m^3.s^{-1}$. For instantaneous discharge of the main tributaries (Alto Madre de Dios, Manù, Chiribi and Colorado) that were measured or calculated during the 2013 and 2019 sampling trip, we use values from previous studies (34, 35).

Calculation of uncertainty is done by a Monte Carlo simulation (run 10 000 times for each watershed). As the calculated distributions follow skewed rather than normal distributions, we report the median value (50th percentile) with the uncertainty range defined by the 16th and 84th percentiles (equivalent to 68% of the entire population; SI Appendix). Comparison between the various methods shows good agreement between the different methods for the different sites within uncertainties (Dataset S3). The third method gives larger uncertainty compared to methods 1 and 2. This could reflect the lower number of samples used, the uncertainty on the discharge measurement or an imbalance between the discharge during the 1968-1982 period and the 2010-2020 period. When quantifying OC_{petro} oxidation fluxes from the dissolved Re flux for all sites, we use the second method (discharge-weighted $[Re]_{diss}$) when possible and the first method (mean $[Re]_{diss}$) otherwise.

Source partitioning of dissolved rhenium. To quantify the OC_{petro} oxidation flux using dissolved Re, we need to: i) correct for Re inputs from precipitation and/or atmospheric deposition; ii) quantify the Re input from non-OC_{petro} sources (i.e. sulfide, carbonate and silicate minerals). Solutes in precipitation can come from dissolution of sea salts, dust or biogenic particles. The [Re]/[Cl] ratio (~7.5×10^{-5} $pmol.\mu mol^{-1}$) of the ocean is very low (58) compared to the [Re]/[Cl] of rivers from the Madre de Dios. The $[Cl]_{diss}$ in rivers from this study are also low, indicating that the proportion of Re derived from sea salts is very small. While we have only one rainwater sample from the upper Andes, its $[Re]_{diss}$ was below detection limit of the measurement session (< 0.05 $pmol.L^{-1}$), supporting this conclusion. Among all the samples, the lowest measured $[Re]_{diss}$ and [Re]/[Cl] ratio correspond to a lysimeter sample in the Foreland (PER19-38) with values of 0.009 $pmol.L^{-1}$ and 1.4×10^{-3} $pmol.\mu mol^{-1}$ respectively. The [Re]/[Cl] ratio of this sample is ~20 times higher than the [Re]/[Cl] ratio of the ocean. The major element concentration for this sample is in the range of the average composition of rainwater from the Andes from Torres et al., (2015). Hence, we use this sample as representative of the maximum Re/Cl ratio of rainwater. For calculating the proportion of Re derived from each source we used the following mass-balance. For the contribution of the rain:

$$[\mathrm{Re}]_{\mathrm{rain}} = \left(\frac{\mathrm{Re}}{\mathrm{Cl}}\right)_{\mathrm{rain}} \times [\mathrm{Cl}]_{\mathrm{cycl}} \qquad \textbf{[1]}$$

Where $(Re/Cl)_{rain}$ is the proposed elemental ratio between Re and the Cl in the rain (1.4×10^{-3} $pmol.\mu mol^{-1}$) and $[Cl]_{cycl}$ is the cyclic chlorine concentration. Since the marine evaporite contribution is small or negligible in the Madre de Dios catchment (23, 29), we consider that $[Cl]_{cycl} = [Cl]_{riv}$. The concentration of any element X corrected for rainwater and evaporite inputs is referred as "[X*]". We find that the proportion of riverine Re deriving from rainfall is negligible, being generally less than 0.5%, with a maximum of 6%. For SO_4 rain concentration we use a (SO_4/Cl) value of 0.53 corresponding to the median value of precipitation data from Torres et al., (2015). This value is only slightly lower than the lowest (SO_4/Cl) measured in our dataset (sample PER19-38, value of 0.60).

We then move to quantify the proportion of dissolved rhenium derived from OC_{petro} oxidation relative to other potential Re sources (sulfides, silicates, carbonates). Previous work has suggested carbonates are not a major source of dissolved Re (18). If the Re/Ca of carbonates is ~5×10^{-5} $pmol.mol^{-1}$ (18), <1% of total dissolved Re in the studied rivers here can be accounted for by carbonate weathering (a maximum proportion using this Re/Ca ratio and assuming all dissolved Ca in the Madre de Dios catchments is derived from carbonates). We therefore follow the approach developed in Horan et al., (2019), that uses the $(Re/SO_4)^*$ and $(Re/Na)^*$ ratio to characterized Re input from sulfides, silicates and OC_{petro}.

Sulfides have low Re/S (Miller et al., 2011) and silicates low Re/Na relative to OC_{petro} (Horan et al., 2019) and both Na and SO_4 are conservative soluble species in the Madre de Dios catchment (Baronas et al., 2017; Torres et al., 2017; Burt et al., 2021). Assuming that all the $[SO_4^{2-}*]$ is derived from pyrite oxidation (i.e. no evaporite contribution, Torres et al., 2016), we estimate the Re concentration derived from sulfide oxidation:

$$[\mathrm{Re}]_{\mathrm{diss.sulfides}} = \left(\frac{\mathrm{Re}}{\mathrm{SO_4^{2-}}}\right)_{\mathrm{sulfides}} \times [\mathrm{SO_4^{2-}} *] \qquad \textbf{[2]}$$

Where $(Re/SO_4^{2-})_{sulfides}$ is the sulfide composition. Then we can determine the concentration of Re deriving from silicate weathering ($[Re]_{diss\cdot sil}$) using sodium and assuming that all the [Na*] is derived from silicate weathering:

$$[\mathrm{Re}]_{\mathrm{diss.sil}} = \left(\frac{\mathrm{Re}}{\mathrm{Na}}\right)_{\mathrm{silicates}} \times [\mathrm{Na} *] \qquad \textbf{[3]}$$

Where $(Re/Na)_{sil}$ is the silicate signature. Then we attribute the excess Re to the oxidation of OC_{petro}, calculated as:

$$[\mathrm{Re}]_{\mathrm{diss.OC}} = [\mathrm{Re} *] - [\mathrm{Re}]_{\mathrm{diss.sulfides}} - [\mathrm{Re}]_{\mathrm{diss.sil}} \qquad \textbf{[4]}$$

In analogy with studies on silicate and carbonate weathering, we use small tributaries (e.g. Gaillardet et al., 1997; Galy and France-Lanord, 1999) and/or sediment composition (23, 44) to constrain local weathering end-members $[Re]/[SO_4]$ and [Re]/[Na] ratio values (20). Small Andean tributaries draining sulfur-rich metasedimentary rocks display two orders of magnitude variability in $[Re]/[SO_4^*]$ and $[Re]/[Na^*]$ ratios and are positively correlated. Several Andean rivers with low $[Re]/[SO_4^*]$ values (Fig. 3) have similar composition to the median Re/S values of pyrite from the literature ($1.8^{+4.2}/_{-1.7}$ $\times10^{-3}$ pmol.µmol^{-1}, Miller et al., 2011) with the lowest $[Re]/[SO_4^{2-}]$ ratio corresponding to a lysimeter sample (PER19-97) in the riparian area of a small catchment ($[Re]^*/[SO_4^{2-}]^* = 2.2\times10^{-4}$ pmol.µmol^{-1}) and a river sample (r2400) from another small catchment in the Andes ($[Re]^*/[SO_4^{2-}]^* = 4.8\times10^{-4}$ pmol.µmol^{-1}). They both have high SO_4 concentration indicating a high rate of sulfide oxidation. The $[Re]/[SO_4^*]$ ratio of these samples is similar to the sulfide-oxidation rich sample in the Mackenzie basin (Horan et al., 2019). Hence, this suggests that the Re and SO_4 composition of these rivers is dominated by sulfide oxidation of pyrite and that they can be used as end-member values for $(Re/SO_4)_{sulfides}$. The lowest $(Re/SO_4)^*$ value (2.2×10^{-4} pmol.µmol^{-1}) measured here could represent the most "pure" sulfide oxidation end-member and higher $[Re]/[SO_4^*]$ for other rivers would be explained by a small contribution of Re from rock organic carbon oxidation. Alternatively, it is possible that the Re/S from the local bedrock is variable and explains the range of $[Re]/[SO_4^*]$ observed in rivers dominated by sulfide oxidation. A third possibility is that the very low $[Re]/[SO_4^*]$ and $[Re]/[Na^*]$ of some samples is due to non-conservative behavior and removal of dissolved Re because some of these rivers have low pH values (as low as 3.5) and ReO_4^- is less stable under acidic conditions (60). However, this cannot explain the low $[Re]/[SO_4^*]$ value of sample PER19-3 (3.5×10^{-3} pmol.µmol^{-1}) which has pH value of 8. Considering the above discussion we consider $(Re/SO_4)_{sulfides}$ ranging from 2×10^{-4} to 4×10^{-3} pmol.µmol^{-1} that encompass the range of $[Re]/[SO_4^*]$ of Andean rivers that we identified as typical of sulfide oxidation.

Rivers draining mostly granites (sulfide-poor and no OC_{petro}) have low Re/Na but an order of magnitude higher $[Re]/[SO_4]$ ratios relative to Andean tributaries draining shales (Fig. 3). Interestingly, rivers and lysimeter samples from the foreland have similar composition as rivers draining granites. For Foreland rivers, especially at low elevations, deeply weathered soils and high weathering intensity probably leads to almost complete oxidation of pyrite due to its fast kinetics, and therefore we expect the chemical composition of those samples to be less influenced by OW of pyrite than Andean rivers. Altogether, rivers draining granite and the foreland have ratios that are inferred to reflect mostly mixing between weathering of silicates and weathering of OC_{rock}. These observations are supported by river bed sediment samples. For Andean rivers, the [Re]/[Na] ratio of river bed sediments is similar to the low [Re]/[Na^*] of small tributaries draining granites (lowest value is 2.2×10^{-3} pmol.µmol $^{-1}$ for sample PER19-26) and of samples from small first-order catchments draining the foreland (lowest value is 1.5×10^{-3} pmol.µmol^{-1} for sample PER19-35). In addition, one rock sample, corresponding to an igneous rock (a granophyre), has a very low [Re]/[Na] ratio of 4.3×10^{-4} pmol.µmol^{-1}, similar to the crystalline rock endmember [Re]/[Na] ratio value in the Himalaya (2×10^{-4} pmol.µmol^{-1}, Ref. 18). Hence, we consider here a [Re]/[Na] ratio between 4×10^{-4} and 2×10^{-3} pmol.µmol^{-1} for silicates, which spans the range of lowest [Re]/[Na] values from local solid and river samples.

Using Eq. (1-4) and the range of above defined $(Re/SO_4)_{sulfides}$ and $(Re/Na)_{silicates}$ values for our study area, we can calculate $[Re]_{diss.OC}$ for each sample. The calculation of $[Re]_{diss.OC}$ is done by a Monte Carlo simulation (run 10 000 times for each river) assuming random distribution of $(Re/SO_4)_{sulfides}$ values between 2×10^{-4} and 4×10^{-3} pmol.mol^{-1} and $(Re/Na)_{silicates}$ values between 4×10^{-4} and 2×10^{-3} pmol.µmol^{-1} (SI Appendix; Dataset S4). Fractions of dissolved Re derived from OC_{petro} OW ($f_c=[Re]_{diss.OC}/[Re]_{diss}$) are reported in Dataset S3.

Floodplain mass-balance of dissolved Re. The section of the Alto Madre de Dios river between MLC (mountain front) and AMdD (confluence with Manu River) has relatively minimal tributary input. Over three sampling trips, we observe an increase in the Re concentration between MLC and AMdD by 3% (March 2013), 26% (March 2019) and 12% (May 2019). There is also a systematic increase in Re/Na and Re/SO_4 ratio. The Re concentration of sub-Andean tributaries is about 0.8 ppt, which is higher than the Re concentration at MLC and could explain part of the observed increase. The contribution of water and weathering inputs from sub-Andean-foreland tributaries can be assessed using δD and $\delta^{18}O$ since tributaries (PER19-53, Rio Carbon, Rio Pini Pini) have higher δD (-54.9 to -70.2‰) and $\delta^{18}O$ values (-8.2 to -10.4 ‰) compared to the Alto Madre de Dios at MLC (δD ~ -72.5‰ and $\delta^{18}O$ ~ -10.6‰). The δD and $\delta^{18}O$ of the Alto Madre de Dios does not change significantly which indicates that any Re contribution from these tributaries is too small to explain the observed 26% increase in Re concentration in 2019. Therefore, we conclude that this increase is due to ongoing OC_{petro} oxidation of sediment during transit and/or within the floodplain between MLC and AMdD.

Acknowledgments

This research was funded by an ERC Starting Grant – ROC-CO2 (678779) to R. G. Hilton, by a European Union COFUND/Durham Junior Research Fellowship (267209) to M. Dellinger and by a National Science Foundation award EAR-1455352 to A.J. West. We thank Amazon Journeys Nature Lodges and Amazon Conservation Association (Peru) for field support. We thank Martin West for laboratory support in Durham and we thank Julien Bouchez for providing the two Madre de dios samples collected at Riberalta. We thank William Santini for discussions on existing discharge data. We thank Kim Genuite for his help in designing figure 4.

References

1. R. A. Berner, A. C. Lasaga, R. M. Garrels, The carbonate-silicate geochemical cycle and its effect on atmospheric carbon dioxide over the past 100 million years. *Am. J. Sci* **283**, 641–683 (1983).
2. M. E. Raymo, W. F. Ruddiman, P. N. Froelich, Influence of late Cenozoic mountain building on ocean geochemical cycles. *Geology* **16**, 649–653 (1988).
3. R. G. Hilton, A. J. West, Mountains, erosion and the carbon cycle. *Nature Reviews Earth & Environment* **1**, 284–299 (2020).
4. K. Horan, *et al.*, Mountain glaciation drives rapid oxidation of rock-bound organic carbon. *Science Advances* **3**, e1701107 (2017).
5. M. A. Torres, A. J. West, G. Li, Sulphide oxidation and carbonate dissolution as a source of CO2 over geological timescales. *Nature* **507**, 346–349 (2014).
6. R. A. Berner, Biogeochemical cycles of carbon and sulfur and their effect on

atmospheric oxygen over phanerozoic time. *Global and Planetary Change* **1**, 97–122 (1989).

7. E. W. Bolton, R. A. Berner, S. T. Petsch, The Weathering of Sedimentary Organic Matter as a Control on Atmospheric O2: II. Theoretical Modeling. *Am J Sci* **306**, 575–615 (2006).

8. D. Calmels, J. Gaillardet, A. Brenot, C. France-Lanord, Sustained sulfide oxidation by physical erosion processes in the Mackenzie River basin: Climatic perspectives. *Geology* **35**, 1003–1006 (2007).

9. J. Spence, K. Telmer, The role of sulfur in chemical weathering and atmospheric CO2 fluxes: Evidence from major ions, $\delta^{13}C_{DIC}$, and $\delta^{34}S_{SO4}$ in rivers of the Canadian Cordillera. *Geochimica et Cosmochimica Acta* **69**, 5441–5458 (2005).

10. J. Bouchez, *et al.*, Oxidation of petrogenic organic carbon in the Amazon floodplain as a source of atmospheric CO_2. *Geology* **38**, 255–258 (2010).

11. K. E. Clark, *et al.*, Erosion of organic carbon from the Andes and its effects on ecosystem carbon dioxide balance. *Journal of Geophysical Research: Biogeosciences* **122**, 449–469 (2017).

12. Y. Copard, P. Amiotte-Suchet, C. Di-Giovanni, Storage and release of fossil organic carbon related to weathering of sedimentary rocks. *Earth and Planetary Science Letters* **258**, 345–357 (2007).

13. V. Galy, B. Peucker-Ehrenbrink, T. Eglinton, Global carbon export from the terrestrial biosphere controlled by erosion. *Nature* **521**, 204–207 (2015).

14. V. Galy, O. Beyssac, C. France-Lanord, T. Eglinton, Recycling of Graphite During Himalayan Erosion: A Geological Stabilization of Carbon in the Crust. *Science* **322**, 943–945 (2008).

15. E. L. Leithold, N. E. Blair, D. W. Perkey, Geomorphologic controls on the age of particulate organic carbon from small mountainous and upland rivers. *Global Biogeochemical Cycles* **20** (2006).

16. R. B. Sparkes, N. Hovius, A. Galy, J. T. Liu, Survival of graphitized petrogenic organic carbon through multiple erosional cycles. *Earth and Planetary Science Letters* **531**, 115992 (2020).

17. R. G. Hilton, J. Gaillardet, D. Calmels, J.-L. Birck, Geological respiration of a mountain belt revealed by the trace element rhenium. *Earth and Planetary Science Letters* **403**, 27–36 (2014).

18. T. K. Dalai, S. K. Singh, J. R. Trivedi, S. Krishnaswami, Dissolved rhenium in the Yamuna river system and the Ganga in the Himalaya: role of black shale weathering on the budgets of Re, Os, and U in rivers and CO2 in the atmosphere. *Geochimica et Cosmochimica Acta* **66**, 29–43 (2002).

19. R. G. Hilton, *et al.*, Concentration-Discharge Relationships of Dissolved Rhenium in Alpine Catchments Reveal Its Use as a Tracer of Oxidative Weathering. *Water Resources Research* **57**, e2021WR029844 (2021).

20. K. Horan, *et al.*, Carbon dioxide emissions by rock organic carbon oxidation and the net geochemical carbon budget of the Mackenzie River Basin. *Am J Sci* **319**, 473–499 (2019).

21. G. Soulet, *et al.*, Temperature control on CO2 emissions from the weathering of sedimentary rocks. *Nat. Geosci.*, 1–7 (2021).

22. T. M. Blattmann, *et al.*, Sulphuric acid-mediated weathering on Taiwan buffers geological atmospheric carbon sinks. *Scientific Reports* **9**, 2945 (2019).

23. M. A. Torres, *et al.*, The acid and alkalinity budgets of weathering in the Andes–Amazon system: Insights into the erosional control of global biogeochemical cycles. *Earth and Planetary Science Letters* **450**, 381–391 (2016).

24. A. Bufe, *et al.*, Co-variation of silicate, carbonate and sulfide weathering drives CO 2 release with erosion. *Nature Geoscience* **14**, 211–216 (2021).

25. J. D. Hemingway, *et al.*, Microbial oxidation of lithospheric organic carbon in rapidly eroding tropical mountain soils. *Science* **360**, 209–212 (2018).

26. R. G. Hilton, A. Galy, N. Hovius, M.-J. Horng, H. Chen, Efficient transport of fossil organic carbon to the ocean by steep mountain rivers: An orogenic carbon sequestration mechanism. *Geology* **39**, 71–74 (2011).

27. T. Salles, *et al.*, Hundred million years of landscape dynamics from catchment to global scale. *Science* **379**, 918–923 (2023).

28. Z. Yu, C. Colin, F. Bassinot, S. Wan, G. Bayon, Climate-Driven Weathering Shifts Between Highlands and Floodplains. *Geochemistry, Geophysics, Geosystems* **21**, e2020GC008936 (2020).

29. M. Torres, A. Joshua West, K. E. Clark, Geomorphic regime modulates hydrologic control of chemical weathering in the Andes-Amazon. *Geochimica et Cosmochimica Acta* (2015) https:/doi.org/10.1016/j.gca.2015.06.007 (July 4, 2015).

30. M. Thieme, *et al.*, Freshwater conservation planning in data-poor areas: An example from a remote Amazon basin (Madre de Dios River, Peru and Bolivia). *Biological Conservation* **135**, 484–501 (2007).

31. J. C. Espinoza, *et al.*, Rainfall hotspots over the southern tropical Andes: Spatial distribution, rainfall intensity, and relations with large-scale atmospheric circulation. *Water Resources Research* **51**, 3459–3475 (2015).

32. J. Rapp, M. Silman, Diurnal, seasonal, and altitudinal trends in microclimate across a tropical montane cloud forest. *Climate Research* **55**, 17–32 (2012).

33. K. E. Clark, *et al.*, The hydrological regime of a forested tropical Andean catchment. *Hydrol. Earth Syst. Sci.* **18**, 5377–5397 (2014).

34. M. A. Torres, Baronas J. Jotautas, Clark Kathryn E., Feakins Sarah J., West A. Joshua, Mixing as a driver of temporal variations in river hydrochemistry: 1. Insights from conservative tracers in the Andes-Amazon transition. *Water Resources Research* **53**, 3102–3119 (2017).

35. E. I. Burt, *et al.*, Conservative transport of dissolved sulfate across the Rio Madre de Dios floodplain in Peru. *Geology* (2021) https:/doi.org/10.1130/G48997.1 (May 19, 2021).

36. E. Burt, D. H. Coayla Rimachi, A. J. Ccahuana Quispe, A. J. West, Hydroclimate and bedrock permeability determine young water fractions in streamflow across the tropical Andes mountains and Amazon floodplain. *Hydrology and Earth System Sciences Discussions*, 1–27 (2022).

37. P. Vauchel, *et al.*, A reassessment of the suspended sediment load in the Madeira River basin from the Andes of Peru and Bolivia to the Amazon River in Brazil, based on 10years of data from the HYBAM monitoring programme. *Journal of Hydrology* **553**, 35–48 (2017).

38. J. J. Baronas, M. A. Torres, K. E. Clark, A. J. West, Mixing as a driver of temporal variations in river hydrochemistry. Part 2: Major and trace element concentration dynamics in the Andes-Amazon transition. *Water Resour. Res.*, n/a-n/a (2017).

39. M. S. Wu, A. J. West, S. J. Feakins, Tropical soil profiles reveal the fate of plant wax biomarkers during soil storage. *Organic Geochemistry* **128**, 1–15 (2019).

40. L. Märki, *et al.*, An unshakable carbon budget for the Himalaya. *Nat. Geosci.*, 1–6 (2021).

41. C. A. Miller, B. Peucker-Ehrenbrink, B. D. Walker, F. Marcantonio, Re-assessing the surface cycling of molybdenum and rhenium. *Geochimica et Cosmochimica Acta* **75**, 7146–7179 (2011).

42. J. Gaillardet, B. Dupré, P. Louvat, C. J. Allègre, Global silicate weathering and CO2 consumption rates deduced from the chemistry of large rivers. *Chemical Geology* **159**, 3–30 (1999).

43. A. Galy, C. France-Lanord, Weathering processes in the Ganges–Brahmaputra basin and the riverine alkalinity budget. *Chemical Geology* **159**, 31–60 (1999).

44. M. J. Bickle, E. Tipper, A. Galy, H. Chapman, N. Harris, On discrimination between carbonate and silicate inputs to Himalayan rivers. *Am J Sci* **315**, 120–166 (2015).

45. L. Ghazi, M. Goñi, B. A. Haley, J. M. Muratli, J. C. Pett-Ridge, Concentration-runoff relationships of contrasting small mountainous rivers in the Pacific Northwest, USA: Insights into the weathering of rhenium relative to other weathering products. *Geochimica et Cosmochimica Acta* **337**, 106–122 (2022).

46. W. Rahaman, S. K. Singh, A. D. Shukla, Rhenium in Indian rivers: Sources, fluxes, and contribution to oceanic budget. *Geochem. Geophys. Geosyst.* **13**, Q08019 (2012).

47. K. E. Clark, *et al.*, Storm-triggered landslides in the Peruvian Andes and implications for topography, carbon cycles, and biodiversity. *Earth Surface Dynamics* **4**, 47–70 (2016).

48. X. Gu, S. L. Brantley, How Particle Size Influences Oxidation of Ancient Organic Matter during Weathering of Black Shale. *ACS Earth Space Chem.* (2022) https:/doi.org/10.1021/acsearthspacechem.1c00442 (June 6, 2022).

49. M. A. Torres, *et al.*, Model predictions of long-lived storage of organic carbon in river deposits. *Earth Surface Dynamics* **5**, 711–730 (2017).

50. A. Dosseto, B. Bourdon, J. Gaillardet, L. Maurice-Bourgoin, C. J. Allegre, Weathering and transport of sediments in the Bolivian Andes: Time constraints from uranium-series isotopes. *Earth and Planetary Science Letters* **248**, 759–771 (2006).

51. J. A. Constantine, T. Dunne, J. Ahmed, C. Legleiter, E. D. Lazarus, Sediment supply as a driver of river meandering and floodplain evolution in the Amazon Basin. *Nature Geosci* advance online publication (2014).

52. J. S. Scheingross, *et al.*, Preservation of organic carbon during active fluvial transport and particle abrasion. *Geology* **47**, 958–962 (2019).

53. J. S. Scheingross, *et al.*, The fate of fluvially-deposited organic carbon during transient floodplain storage. *Earth and Planetary Science Letters* **561**, 116822 (2021).

54. J.-S. Moquet, *et al.*, Chemical weathering and atmospheric/soil CO2 uptake in the Andean and Foreland Amazon basins. *Chemical Geology* **287**, 1–26 (2011).

55. M. Dellinger, R. G. Hilton, G. M. Nowell, Measurements of rhenium isotopic composition in low-abundance samples. *J. Anal. At. Spectrom.* **35**, 377–387 (2020).

56. S. Moon, C. P. Chamberlain, G. E. Hilley, New estimates of silicate weathering rates and their uncertainties in global rivers. *Geochimica et Cosmochimica Acta* **134**, 257–274 (2014).

57. N. Abastos Lara, “Balance hidrico superficial de la cuenca del rio Madre de Dios : Amazonia, Bolivia, Peru” (PHICAB, 1987).

58. D. Colodner, *et al.*, The geochemical cycle of rhenium: a reconnaissance. *Earth and Planetary Science Letters* **117**, 205–221 (1993).

59. J. Gaillardet, B. Dupre, C. J. Allegre, P. Négrel, Chemical and physical denudation in the Amazon River Basin. *Chemical Geology* **142**, 141–173 (1997).

60. D. G. Brookins, Rhenium as analog for fissiogenic technetium: Eh-pH diagram (25°C, 1 bar) constraints. *Applied Geochemistry* **1**, 513–517 (1986).

Figures

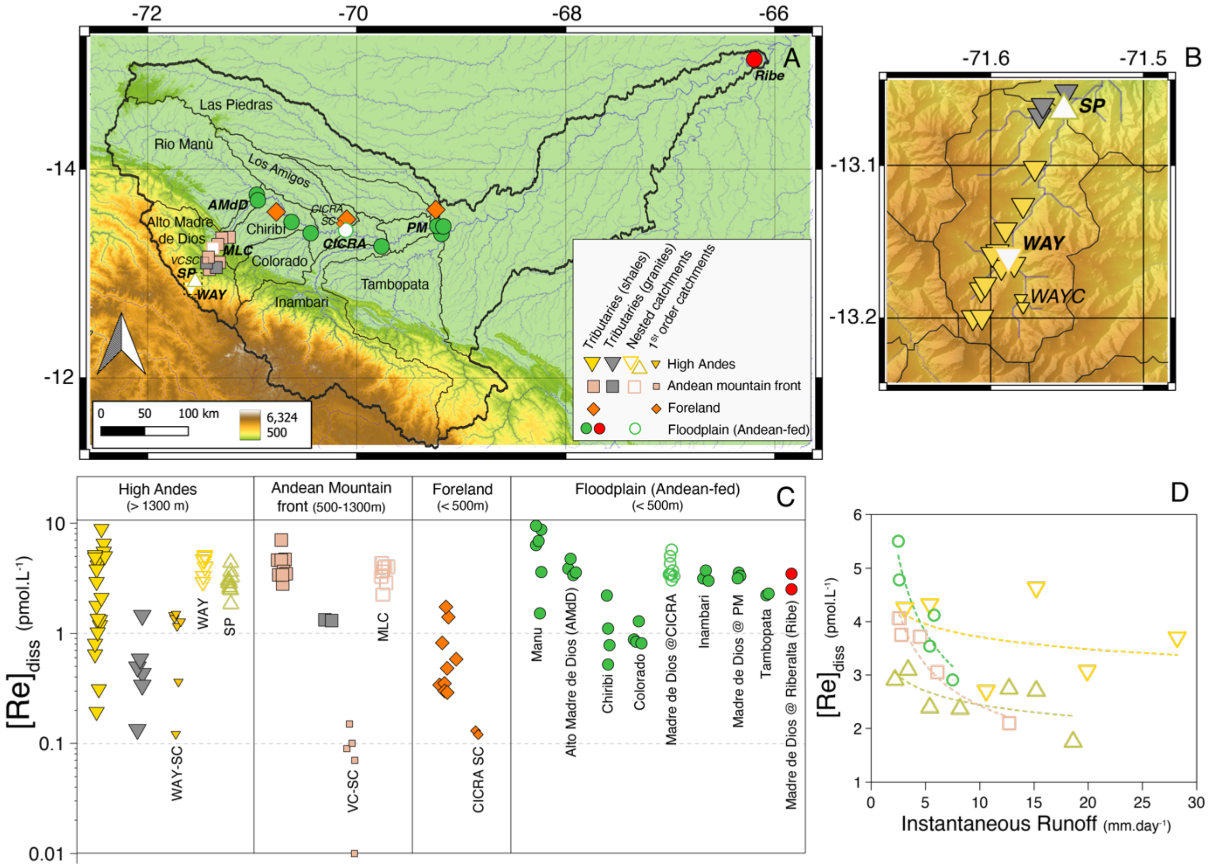

Figure 1. (A) Map of the Madre de Dios River basin with the location of the samples from this study. (B) Inset showing the location of the samples in the High Andes. (C) Re concentration (in pmol.L^{-1}) in the various geomorphic settings for all river samples from this study. The $[\mathrm{Re}]_{\mathrm{diss}}$ from the two hot springs samples are not shown. (D) $[\mathrm{Re}]_{\mathrm{diss}}$ versus instantaneous runoff W (water discharge normalized by catchment area, mm day^{-1}) at the time of sampling for the main nested catchments of this study (WAY, SP, MLC and CICRA).

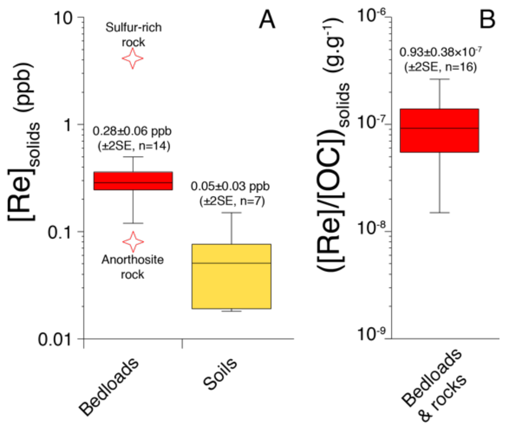

Figure 2. (A) Rhenium concentration in solids ($[Re]_{solids}$): rock samples (red stars), bedloads (red box) and soils (yellow box). The middle line in boxes is the average value, upper and lower box limits correspond to the ±2SE values, the upper and higher bars represent extreme data points. (B) Average ± 2SE and extreme values of the [Re]/[OC] ratio in bedloads and rocks.

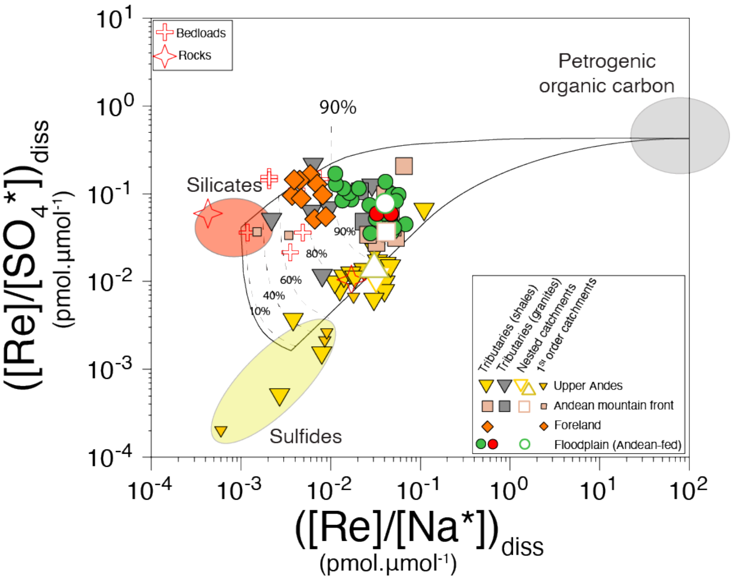

Figure 3. Rhenium to sodium, [Re]/[Na*], and rhenium to sulfate, [Re]/[SO_4*], ratios (pmol µmol^{-1}) for river waters from this study (High Andes = triangles; Andean Mountain front = square; Foreland = diamond; circles = Foreland-Floodplains). For the four nested-catchments, only the average values are represented. The red crosses correspond to the river sediments (bedloads) and bedrocks from the Kosnipata River basin. The shaded ovals show the ranges of elemental ratios associated with the rock weathering end-members (sulfides, silicates and OC_{petro}). The lines correspond to the mixing proportions between the rock weathering end-members, with the average proportion of Re derived from OC_{petro} weathering shown (in %).

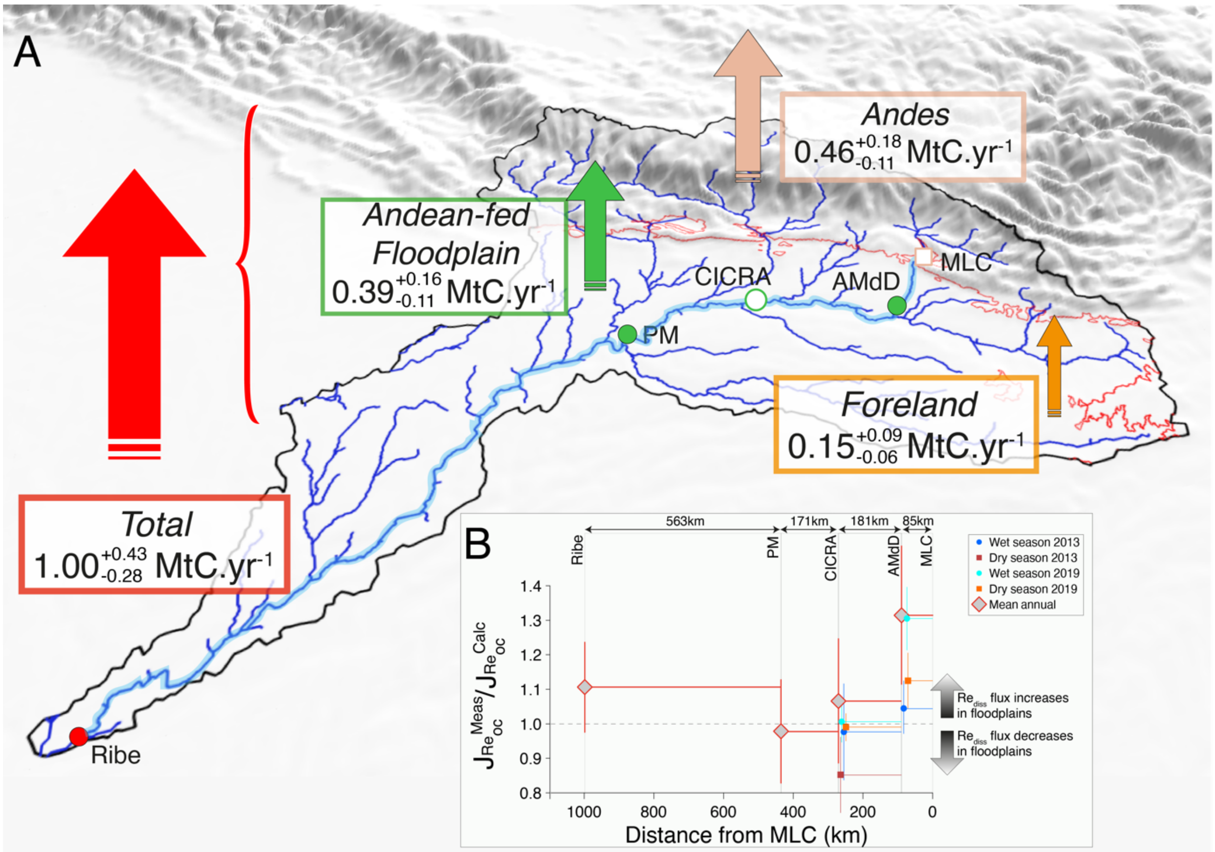

Figure 4. (A) Estimated net contribution (vertical arrows) of each geomorphic zones to the total flux of OC$_{petro}$ oxidation and associated CO$_2$ release at the scale of the whole Madre de Dios River basin. MLC=Mountain Front, AMdD=Alto Madre de Dios, PM=Madre de Dios at Puerto Maldonado, Ribe=Madre de Dios at Riberalta. The red squiggly line corresponds to the 500m elevation. (B) Ratio between the measured dissolved rhenium flux derived from OC$_{petro}$ oxidation ($J_{Re\text{-}OC}^{meas}$) and the predicted flux ($J_{Re\text{-}OC}^{calc}$) using the tributary mixing model (SI Appendix) as a function of the channel distance from MLC. A value >1 can be interpreted as OC$_{petro}$ oxidation in the floodplain. Vertical bars represent the uncertainties. This studied floodplain transect correspond to the channel highlighted in light blue on panel A.